Appl. Numer. Math. 207 (2025) 608–620

Contents lists available at ScienceDirect

Applied Numerical Mathematics

journal homepage: www.elsevier.com/locate/apnum

Research Paper

A fractional order SIR model describing hesitancy to the COVID-19 vaccination

Constantino Caetano [a,*], Luísa Morgado [b], Pedro Lima [c], Niel Hens [d,e], Baltazar Nunes [f]

[a] Instituto Nacional de Saúde Doutor Ricardo Jorge, Departamento de Epidemiologia, Lisboa, 1600-609, Portugal
[b] University of Trás-os-Montes e Alto Douro (UTAD), Department of Mathematics, Portugal, Vila Real, 5000-801, Portugal
[c] Instituto Superior Técnico, Department of Mathematics, Lisboa, 1049-001, Portugal
[d] Interuniversity Institute for Biostatistics and Statistical Bioinformatics, Data Science Institute, Hasselt University, Hasselt, Belgium
[e] Centre for Health Economic Research and Modelling Infectious Diseases, Vaccine and Infectious Disease Institute, University of Antwerp, Antwerp, Belgium
[f] NOVA National School of Public Health, Public Health Research Center, Universidade NOVA de Lisboa, Lisboa, Portugal

ARTICLE INFO

MSC:
26A33
62N02
92B05
92B15

Keywords:
Fractional derivatives
SIR model
Vaccine hesitancy
COVID-19

ABSTRACT

This study introduces a SIR (Susceptible-Infectious-Recovered) model using fractional derivatives to assess the population's hesitancy to the COVID-19 vaccination campaign in Portugal. Leveraging the framework developed by Angstmann [1], our approach incorporates fractional derivatives to best describe the nuanced dynamics of the vaccination process. We begin by examining the qualitative properties of the proposed model. To substantiate the inclusion of fractional derivatives, empirical data along with statistical criteria are applied. Numerical simulations are performed to compare both integer and fractional order models. An epidemiological interpretation for the fractional order of the model is provided, in the context of a vaccination campaign.

1. Introduction

Fractional calculus is a field that deals with the generalisation of classic integer-order integral and differential operators by considering non-integer integral and derivative orders. Its history begins with a purely mathematical approach; however, more recently, it has found applications in various domains. Fractional operators, unlike their classical counterparts, are not local operators, that is, they carry the history of all previous states of the system. These properties are well-suited to model many problems, such as the viscoelasticity of materials and drug absorption [2–4].

There are several definitions of fractional integral and differential operators, being the Riemann-Liouville integral and the Caputo differential operator the two most common. The Riemann-Liouville integral operator of order $\alpha > 0$, defined on $L_1[a,b]$, is given by

$$J_a^{\alpha} f(x) = \frac{1}{\Gamma(\alpha)} \int_a^x (x-t)^{\alpha-1} f(t)\, dt, \tag{1}$$

* Corresponding author.
E-mail address: constantino.caetano@insa.min-saude.pt (C. Caetano).

https://doi.org/10.1016/j.apnum.2024.10.001
Received 29 February 2024; Received in revised form 20 September 2024; Accepted 1 October 2024

Available online 5 October 2024

where $a < x < b$ and $\Gamma(\alpha)$ corresponds to the Gamma function. This operator arises as a natural generalisation of the Cauchy formula for repeated integration. The Riemann-Liouville derivative of order $\alpha > 0$ is defined by

$$D_a^\alpha f(x) = D^m J_a^{m-\alpha} f(x), \tag{2}$$

where m is a positive integer satisfying $m - 1 < \alpha < m$, and $D^m f(x) \equiv f^{(m)}(x)$, $m \in \mathbb{N}$. When $m = 1$, a differentiation of order $0 < \alpha < 1$ assumes an integration of order $(1 - \alpha)$ followed by differentiation of order 1. This formulation is rarely used in practical applications since, when dealing with initial value problems, initial conditions with non-integer order derivatives are necessary [5]. The Caputo fractional derivative arises as a solution to this problem. It consists of permuting the order of the operators for the Riemann-Liouville derivative, i.e., a differentiation of order 1 followed by an integration of order $(1 - \alpha)$, in the case where $0 < \alpha < 1$. By definition, both differential operators become equivalent to the classic differential operator if the differentiation order is an integer.

Due to its similar properties to classic integer-order operators [5], the Caputo fractional derivative has found widespread applications. In epidemiology of infectious diseases, a common practice involves extending integer-order derivatives in compartmental models by incorporating fractional derivatives of the Caputo type. Here, the fractional order α, typically within the range $]0, 1]$, is considered a free parameter. This framework has been employed to assess the spread of diseases such as Dengue [6,7] and COVID-19 [8–11]. These studies show that the non-locality or memory provided by the Caputo fractional derivative leads to a better fit of the model to data. However, some authors argue against the use of this framework, stating the absence of epidemiological or biological justification for the inclusion of fractional derivatives [12]. Moreover, challenges arise in this formulation, including difficulties in interpreting unit constants and issues related to the conservation of mass. As highlighted in [3,4], the conservation of mass is not guaranteed in a compartmental system if equations with distinct differentiation orders coexist. In this paper we intend to overcome these issues by including, in a non-artificial way, a fractional-order derivative in a COVID-19 model. To that end, we resort to the use of the Mittag-Leffler probability distribution function [13] for the derivation of the model. The survival function linked to the Mittag-Leffler distribution often serves as the solution to linear initial value problems with Caputo derivatives. In [2], the authors show that this function initially exhibits a behaviour akin to the exponential survival function but undergoes a slower decay over time. They argue that these properties may be well-suited for modelling drug absorption in deep tissues.

While the Mittag-Leffler distribution is a generalisation of the exponential distribution, it does not retain the property of memorylessness. This concept is explored in the framework proposed by Angstmann et al. [12]. In this framework, the authors present a method for constructing compartmental models using fractional derivatives. These equations stem from master equations for stochastic processes, with a focus on modelling specific non-Markovian removal processes employing arbitrary continuous probability distributions.

When the Mittag-Leffler probability distribution is chosen to model such processes, Riemann-Liouville derivatives appear on the right-hand side of the equations associated with the flux of the Mittag-Leffler removal process, along with classical first-order derivatives on the left-hand side. The authors emphasise that the Mittag-Leffler distribution exhibits a decreasing hazard function, implying that the rate of particle removal at time t, given its survival up to that moment, diminishes over time, leading to particles being trapped inside the compartment as time progresses.

This framework is also applied in [14], where a SIR model with a Mittag-Leffler recovery process is derived. The authors argue that this approach could be well-suited for diseases with potential chronic infection. The same framework has been used to describe the transmission dynamics of Dengue in [15]. Notably, this fractional framework has an equivalent integral formulation. In fact, the authors in [14] connected this framework to the work of Hethcote et al., where Volterra integral equations of the second kind were employed [16,17]. The integral formulation facilitates the study of the stability of equilibria [16,18], compared to the fractional framework outlined in [12].

In this study, we employ the framework proposed by Angstmann et al. to develop a SIR model that characterises the transmission dynamics of COVID-19, considering the presence of a vaccination process modelled with a Mittag-Leffler probability distribution. Section 2 provides a brief overview of the framework proposed by Angstmann et al. [12]. In Section 3, we derive the model and explore its qualitative properties. The model introduces a non-Markovian process with Mittag-Leffler distribution of waiting times associated with vaccination, resulting in a system with fractional-order derivatives.

Section 4 presents a data study using COVID-19 vaccination data. In this analysis, we utilise model selection statistical criteria to justify the incorporation of the Mittag-Leffler vaccination process into the model. In Section 4.2, we provide some numerical simulations by adapting the numerical approach proposed in [19]. We discuss the obtained results by comparing the fractional-order model with the integer-order one. Specifically, we compare the assumption that the vaccination process is modelled by a Mittag-Leffler distribution instead of an exponential distribution. We end with some conclusions and plans for further investigation.

2. Compartmental models with fractional derivatives

In this section we present a summary of the results detailed in [12] for compartmental models using fractional derivatives, along with important results about the Mittag-Leffler distribution.

The expected number of particles in a single compartmental model at time t is given by

$$\rho(t) = \int_0^t \Phi(t - t_0)\Theta(t, t_0)q(t_0)\, dt_0, \tag{3}$$

with $q(t) = i_0\delta(t-0^+) + q^+(t)$, where i_0 denotes the initial injection of particles at $t=0$, $\delta(t)$ is the delta Dirac function and $q^+(t)$ represents the time-dependent creation of particles [12]. Using this formulation for $q(t)$ we can further write

$$\rho(t) = i_0\Phi(t)\Theta(t,0) + \int_0^t \Phi(t-t_0)\Theta(t,t_0)q^+(t_0)\,dt_0. \tag{4}$$

Function $\Theta(t,t_0)$, $t > t_0 > 0$, represents the survival function associated with the Markovian removal processes and takes the form

$$\Theta(t,t_0) = \exp\left(-\int_{t_0}^t \omega(s)ds\right), \quad t \geq 0, \tag{5}$$

where $\omega(t)$ denotes the total removal rate. This function has the following semi-group property $\Theta(t,t_0) = \Theta(t,u)\Theta(u,t_0)$, $t_0 < u < t$. Function $\Phi(t)$ represents the survival function associated with a non-Markovian removal process. Its form is dependent on the choice of waiting time distribution associated with this process. Function $\rho(t)$ is non-decreasing, non-negative and right continuous at $t=0$ and continuous for all $t > 0$. We also assume $\rho(t) = 0$, $t < 0$.

Markovian processes have no memory, i.e. the removal probability of a particle is only dependent on the current state of the system. In contrast, in a non-Markovian process previous states of the system influence its removal.

The Mittag-Leffler distribution has two parameters, a time scale parameter $\tau > 0$ and a tail parameter (or fractional order) $0 < \alpha \leq 1$. Its survival function is given by

$$\Phi(t) = E_{\alpha,1}(-(t/\tau)^\alpha), \tag{6}$$

where

$$E_{\alpha,\lambda}(t) = \sum_{j=0}^{\infty} \frac{t^j}{\Gamma(j\alpha+\lambda)}, \; t > 0 \tag{7}$$

is the Mittag-Leffler function [5]. The following remark presents some results about the Mittag-Leffler distribution.

Remark. The Mittag-Leffler density function is given by

$$\phi(t) = \frac{t^{\alpha-1}}{\tau^\alpha} E_{\alpha,\alpha}\left(-\left(\frac{t}{\tau}\right)^\alpha\right).$$

The hazard function of a continuous probability distribution can be calculated as

$$h(x) = \lim_{s\to 0} \frac{P(x < X < x+s)}{F(x)\,ds} = \frac{f(x)}{F(x)}, \tag{8}$$

where $F(x)$ and $f(x)$ represent and the cumulative distribution function and density function, respectively. In the setting of a waiting time distribution, it represents the rate at which particles are removed at time t, conditional on having survived up to that moment. In the case of power-law tailed distributions, e.g. the Mittag-Leffler distribution, we have

$$h(t) \approx \frac{\alpha}{t}, \tag{9}$$

as we take $t \to \infty$. The hazard function decreases with time, indicating that the longer a particle is in a compartment, the less likely it is to be removed.

Generalising equation (3) for $k = 1, 2, 3, ..., K$ compartments and computing the associated derivatives, we arrive at a master equation for the ensemble of particles in each compartment:

$$\frac{d\rho_k}{dt} = q_k^+(t) - \omega_k(t)\rho_k(t) - \tau_k^{-\alpha_k}\Theta_k(t,0)D_0^{1-\alpha_k}\left(\frac{\rho_k(t)}{\Theta_k(t,0)}\right). \tag{10}$$

To derive these equations, we employ Laplace transform techniques and assume that $\Phi(t)$ is given by the survival function of the Mittag-Leffler distribution. More details on the derivation of these equations, can be found in [12].

2.1. Numerical method

In this section we briefly summarise a numerical method for compartmental models with fractional derivatives as presented in the previous section. This method was first introduced in [19]. The discrete version of equation (3) can be written as

$$X(n) = \sum_{k=0}^{n} \Xi(n,k)Q(k), \tag{11}$$

which denotes the expected number of particles, at discrete time n, in a single compartment model. Function $\Xi(n,k) = \Theta(n,k)\Phi(n-k)$ represents the probability of surviving both removal processes, where $\Theta(n,k)$ is the survival function associated with the Markovian removal process and $\Phi(n-k)$ represents the survival function associated with the non-Markovian removal process. Function $Q(k)$ represents the influx of particles in the compartment at time step k.

We can generalise this approach to a system with multiple compartments X_i, $i = 1, ..., M$, we can define a $(M+1)\times(M+1)$ flux matrix $\mathcal{Q}$, where M represents the number of compartments. Entry $Q_{i,j}(n)$ describes the flux from compartment i to j at discrete time n. The remaining dimension details the entries and removals not associated with a compartment. The flux balance equation is given by

$$X_i(n) = X_i(n-1) + \sum_{l=1}^{M+1} Q_{l,i}(n) - \sum_{l=1}^{M+1} Q_{i,l}(n), \tag{12}$$

where $\sum_{l=1}^{M+1} Q_{l,i}(n)$ is the column sum of $\mathcal{Q}$, which represents the flux into compartment X_i, $i = 1, ..., M$ and $\sum_{l=1}^{M+1} Q_{i,l}(n)$, the row sum, represents the flux out of X_i. If we assume that a particle may only leave the compartment due to a Markovian process i, if it first survived all Markovian processes $j < i$, and the non-Markovian process is always considered after the Markovian processes, we can write

$$\begin{aligned} Q_{i,l}(n) = &\sum_{k=0}^{n-1}\left(\prod_{j=1}^{M+1}\Theta_{ij}(n-1,k)\Phi_{i,j}(n-1-k)\right)(1-\Theta_{i,j}(n,n-1)) \\ &\times\prod_{j=1}^{l-1}\Theta_{i,j}(n,n-1)\left(\sum_{h=1}^{M+1}Q_{h,i}(k)\right) \\ &+\sum_{k=0}^{n-1}\prod_{j=1}^{M+1}\Theta_{i,j}(n,k)(\Phi_{i,l}(n-1-k)-\phi_{i,l}(n-k))\left(\sum_{h=1}^{M+1}Q_{h,i}(k)\right), \end{aligned} \tag{13}$$

where $\Theta_{i,l}(n,k)$ and $\Phi_{i,l}(n-k)$ represent the Markovian and non-Markovian survival functions associated with the removal process of compartment i into compartment l. Note that $\Phi_{i,l}(n-k) = 1$ for all except one l, at most one non-Markovian transition out of each compartment. It is a necessary assumption in order to write the system of equations (15) to (17) using fractional derivatives. See [19] for more details on the method.

3. A fractional order SIR model

In this section, we develop a SIR compartmental model that incorporates a non-Markovian removal process to describe the vaccination process. The objective is to represent population hesitancy to a vaccination campaign by using a heavy-tail distribution for the waiting times until vaccination, as opposed to the classic light-tailed exponential distribution. We define waiting times until vaccination as the elapsing time since individuals are eligible to be vaccinated until the moment they receive the vaccine. In a later section, we show that the heavy-tail vaccination principle is observed in the COVID-19 vaccination data in Portugal during 2021. We aim to explore how this assumption impacts the evolution of an epidemic.

We will start with the equation for the proportion of susceptible individuals. Let $S(t) = \rho_1(t)$. Then, by equation (10), we can write

$$\frac{dS}{dt} = q_1^+(t) - \omega_1(t)S(t) - \tau^{-\alpha}\Theta_1(t,0)D_0^{1-\alpha}\left(\frac{S(t)}{\Theta_1(t,0)}\right). \tag{14}$$

The waiting times in the susceptible compartment are governed by a non-Markovian process associated with vaccination and Markovian processes associated with natural mortality and infection. We need to specify the Markovian survival function $\Theta_1(t,0)$ and the function that creates new susceptibles $q_1^+(t)$. The term $\tau^{-\alpha}\Theta_1(t,0)D_0^{1-\alpha}\left(\frac{S(t)}{\Theta_1(t,0)}\right)$ represents the outgoing flux of susceptibles associated with vaccination, i.e., the non-Markovian removal process with Mittag-Leffler distributed waiting times. Parameters τ and α are the time scale and fractional order parameters of the Mittag-Leffler distribution. We assume that the rate of births is constant, and newborn individuals are susceptible to infection. Hence,

$$q_1^+(t) = \mu, \quad \mu > 0.$$

The term $\omega_1(t)S(t)$ is the outgoing flux associated with the Markovian removal processes. This removal process includes two possibilities: natural death or infection. Assuming the natural death rate is also $\mu > 0$, we can write $\omega_1(t) = \beta I(t) + \mu$, where $\beta > 0$ represents the transmission rate. Moreover, by equation (5), we have fully specified $\Theta_1(t,0)$, written as

$$\Theta_1(t,t_0) = \exp\left(-\int_{t_0}^{t}\beta I(s) + \mu\, ds\right).$$

We can then write the final differential equation for S as

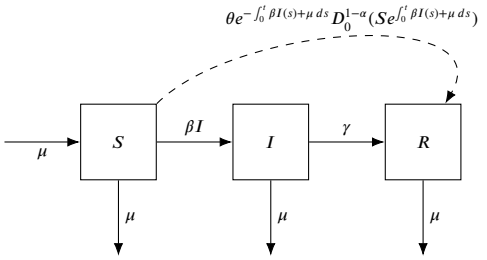

Fig. 1. Diagram of the SIR model with Mittag-Leffler vaccination process. The solid arrows represent Markovian removal processes. The dashed arrow represents the non-Markovian removal process associated with vaccination.

$$\frac{dS}{dt} = \mu - \beta SI - \mu S - \theta e^{-\int_0^t \beta I(s)+\mu\, ds} D_0^{1-\alpha}\left(Se^{\int_0^t \beta I(s)+\mu\, ds}\right). \tag{15}$$

Here, $\theta = \tau^{-\alpha}$ represents the inverse of the time-scale vaccination parameter.

For the equation associated with the proportion of infected $I(t) = \rho_2(t)$, there are no non-Markovian removal processes, leading to the exclusion of the rightmost term in equation (10). However, we still need to specify $q_2^+(t)$ and $\omega_2(t)$. The creation of infectious individuals needs to match the outgoing flux of susceptible individuals due to infection; hence, $q_2^+(t) = \beta S(t)I(t)$. Removals in the infectious compartment can be due to natural death or recovery; thus, $\omega_2(t) = \mu + \gamma$, where $\gamma > 0$ represents the recovery rate. This results in the following differential equation for $I(t)$:

$$\frac{dI}{dt} = \beta SI - (\mu + \gamma)I. \tag{16}$$

Note that this equation is the same as for the classic integer-order version of the SIR model.

We assume that the population is kept constant, i.e., $\frac{dS(t)}{dt} + \frac{dI(t)}{dt} + \frac{dR(t)}{dt} = 0$, and initial conditions are such that $S_0 + I_0 + R_0 = 1$. Hence, we can immediately write the differential equation for $R(t)$ as

$$\frac{dR}{dt} = \gamma I + \theta e^{-\int_0^t \beta I(s)+\mu\, ds} D_0^{1-\alpha}(Se^{\int_0^t \beta I(s)+\mu\, ds}) - \mu R, \tag{17}$$

Vaccinated individuals leave the susceptible group and are considered recovered; thus, we assume that the vaccine confers long-lasting protection against the infection.

The system of equations (15) to (17) reduces to the classic (integer order) SIR model when $\alpha = 1$. A schematic of the complete model is presented. See Fig. 1.

3.1. Equilibria

Given that $R(t) = 1 - I(t) - S(t)$, we need only to study the equations for the $I(t)$ and $S(t)$ groups. The equilibrium points of the ODE referring to the infected are the solutions (S^*, I^*) such that $\frac{dS}{dt} = 0$ and $\frac{dI}{dt} = 0$, leading to

$$0 = \beta SI - (\mu + \gamma)I. \tag{18}$$

Either $I^* = 0$ or $S^* = \frac{\mu+\gamma}{\beta}$. The first will lead to the *disease free equilibrium* and the second to the *endemic equilibrium*, similar to the classic case when $\alpha = 1$.

We start by studying the case where $I^* = 0$. In this case, taking (15) into account,

$$\frac{dS}{dt} = \mu - \mu S - \theta e^{-\mu t} D_0^{1-\alpha}(Se^{\mu t}). \tag{19}$$

Note that the previous equation is a non-autonomous differential equation, hence we study the equilibrium points such that $\lim_{t\to\infty} S(t) = S^*$, taking the limit of (19),

$$0 = \mu - \mu S^* - \theta \lim_{t\to\infty} e^{-\mu t} D_0^{1-\alpha}(S(t)e^{\mu t}).$$

Following the procedure described in [12,14] we arrive at

$$(S_{dfe}, I_{dfe}, R_{dfe}) = \left(\frac{\mu}{\mu + \theta\mu^{1-\alpha}}, 0, 1 - \frac{\mu}{\mu + \theta\mu^{1-\alpha}}\right), \tag{20}$$

Alternatively, using equation (4), we can find the equilibrium solution directly from this integral equation:

$$S(t) = S_0 e^{-\mu t} E_\alpha\left(-\left(\frac{t}{\tau}\right)^\alpha\right) + \int_0^t e^{-\mu(t-t_0)} E_\alpha\left(-\left(\frac{t-t_0}{\tau}\right)^\alpha\right)\mu\, dt_0$$

Taking $t \to \infty$, we have that $e^{-\mu t} E_\alpha\left(-\left(\frac{t}{\tau}\right)^\alpha\right) \to 0$, given that these are the product of survival functions and

$$\mu \int_0^\infty e^{-\mu t} E_\alpha\Big(-\Big(\frac{t}{\tau}\Big)^\alpha\Big)\, dt = \frac{\mu}{\mu + \tau^{-\alpha}\mu^{1-\alpha}}$$

as given by the Laplace transform of the Mittag-Leffler function evaluated at $\mu > 0$.
Note that, we can arrive at the disease free equilibrium for the integer order SIR model by considering $\alpha = 1$ in equation (20):

$$(S_{dfe}, I_{dfe}, R_{dfe}) = \left(\frac{\mu}{\mu+\theta}, 0, 1 - \frac{\mu}{\mu+\theta}\right).$$

Finding the *endemic equilibrium* is not as trivial, since the removal rate associated with the Markovian process $\omega(t) = \beta I(t) + \mu$ is time dependent. However, if $\lim_{t\to\infty} I(t) = I^*$ then $\omega(t) \to \beta I^* + \mu$. If we write $f(S, I, t) = \frac{dS}{dt}$ then we want to find the time-independent solutions such that

$$\lim_{t\to\infty} f(S^*, I^*, t) = 0. \tag{21}$$

In *endemic equilibrium* we have that $S^* = \frac{\mu+\gamma}{\beta}$; then, substituting in (21) we arrive at

$$\beta I^* + \mu + \theta(\beta I^* + \mu)^{1-\alpha} - \frac{\mu\beta}{\mu+\gamma} = 0. \tag{22}$$

Again we use the procedure described in [12,14] to arrive at this conclusion. Similar to the previous result for the *disease free equilibrium*, if we assume $\alpha = 1$ in (22) then

$$I^* = \frac{\mu}{\mu+\gamma} - \frac{\mu+\theta}{\beta},$$

which corresponds to the *endemic equilibrium* of the classic integer order SIR model. It is not possible to obtain an explicit expression for I^* from (22), when $0 < \alpha < 1$. Considering a first order approximation around $I^* = 0$,

$$(\beta I^* + \mu)^{1-\alpha} = \mu^{1-\alpha} + I^*(1-\alpha)\mu^{-\alpha}\beta + R_2, \tag{23}$$

if we ignore R_2 and incorporate (23) into (22) while taking $\alpha = 1$ we still recover the endemic equilibrium for the integer order SIR model, and for $0 < \alpha < 1$ we have

$$I^* = \frac{\mu\beta - \mu(\mu+\gamma)S_{dfe}^{-1}}{(\mu+\gamma)\beta(1-\alpha)(\theta\mu^{-\alpha})}.$$

Note also that the denominator is always positive, hence $I^* > 0$ when

$$\mathcal{R} = \frac{\beta}{\mu+\gamma} S_{dfe} > 1, \tag{24}$$

which matches the exact same qualitative result for the integer order SIR model. Note that here $\mathcal{R}$ represents the reproduction number, i.e., the average number of infections caused by an infected individual during the infectious period if the susceptible population is in *disease free equilibrium*. In the following sections we will perform numerical simulations to illustrate the behaviour of the system with respect to the stability of the equilibrium states found here. However, we expect a similar behaviour as obtained for the classical setting, especially if we take $\alpha \approx 1$, i.e. the system will tend to the disease free equilibrium as $t \to \infty$ if $\mathcal{R} < 1$ and it will tend towards the endemic equilibrium when $\mathcal{R} > 1$.

It is also interesting to study how the fractional order affects the reproduction number. This can be done by computing the sensitivity of $\mathcal{R}$ with respect to α. Note that the fractional order only affects the term in $\mathcal{R}$ associated with S_{dfe}. This is expected since the vaccination process considered does not interfere directly with transmission; it simply removes individuals from the pool of susceptibles. The sensitivity of S_{dfe} with respect to α is given as

$$\frac{dS_{dfe}}{d\alpha} = \frac{\log(\tau\mu)}{(1+(\tau\mu)^{-\alpha})^2(\tau\mu)^\alpha}. \tag{25}$$

This expression is negative when $\tau\mu < 1$. Note that τ and μ are not given in the same unit: τ is in time units, and μ is in time^{-1} units. Let $\theta_1 = \frac{1}{\tau}$. Then, (25) is negative when $\theta_1 > \mu$, i.e., when the vaccination rate[1] is higher than the mortality/birth rate. This result suggests that, if all other parameters remain equal, lowering the fractional order parameter results in a higher proportion of susceptibles at the *disease-free equilibrium*, thus a greater reproduction number. This can be explained by equation (9): a lower fractional order will result in a heavier tail for the distribution of times until vaccination, i.e., a lower vaccination (hazard) rate as time goes on. This implies that more individuals are trapped in the susceptible compartment and consequently are more likely to be infected. The previous result suggests that the fractional order is linked to the population hesitancy to get vaccinated; a lower

[1] This parameter can only be interpreted as a rate when $\alpha = 1$, however, it still represents the speed at which the vaccination process occurs.

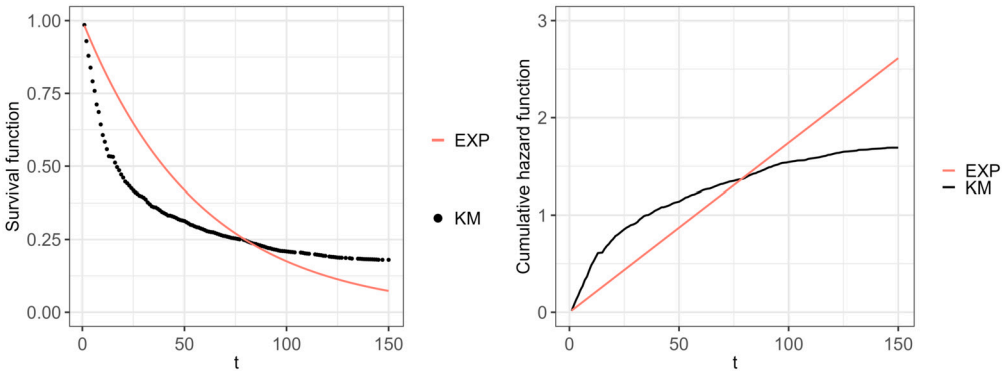

Fig. 2. Empirical and exponential survival functions for the time until vaccination (left). Empirical and exponential cumulative hazard functions (right). Cumulative hazard functions are given by $\Lambda(t) = -\log(\Phi(t))$. (For interpretation of the colours in the figure(s), the reader is referred to the web version of this article.)

fractional order implies more hesitancy to get vaccinated. The case when $\mu \geq \theta_1$ is not of interest since the vaccination process always occurs faster than the renewal of the population.

4. Measuring the fractional order

In this section, we test the hypothesis that the time until vaccination is best modelled by a heavy-tail probability distribution law. We start by describing the data.

Individual vaccination waiting times (time since being eligible to the vaccine and receiving it) for the COVID-19 vaccination campaign in Portugal were obtained from the Portuguese health registry data. The first vaccination campaign occurred in three different phases, encompassing different eligibility criteria. We choose to evaluate the second phase that started in April 2021, where the eligible groups consisted of those between 50-64 years old with comorbidities, along with those older than 65 years of age.

We started our analysis on May 1, 2021. Although eligibility for these groups began in early April, most vaccinations occurred between May and September 2021 [1]. We also restrict our population to those above 65 years of age and assume a 5-month follow-up period. To reduce computational costs, we randomly sampled $m = 5000$ waiting times from this pool of individuals. Waiting times for individuals not yet vaccinated by the end of the follow-up count as right-censored data. No loss to follow-up occurs during the period. Observations consist of $x_i = \min(t_i, c)$, where t_i, $i = 1, 2, ..., m$ are realisations of the random variable T which describes the time until vaccination, and c denotes the end of the follow-up. Waiting times are censored if $t_i > c$, uncensored otherwise. We denote v_i as the Boolean variable describing the observed times, i.e., $v_i = 0$ if $t_i > c$ and $v_i = 1$ otherwise. Computations were performed using the `R` language and environment for statistical computing and graphics [20] and associated packages.

The empirical survival function for the times until vaccination can be computed using the Kaplan-Meier estimator [21] and is presented in Figs. 2 and 3. We observe that the empirical survival function for the time until vaccination displays a heavy tail. After 150 days, 18% of individuals have not yet received the vaccine.

Next, we want to fit these waiting times to a parametric model, i.e., the Mittag-Leffler probability distribution. Inference on α and τ is performed via the likelihood function [22]

$$L(\tau, \alpha) = \prod_{i=1}^{m} \phi(x_i; \tau, \alpha)^{v_i} \Phi(t_i; \tau, \alpha)^{1-v_i}, \tag{26}$$

where $\Phi(t)$ denotes the survival function and $\phi(t)$ the density function. The maximum likelihood estimates of τ and α are the values that maximise (26). We first consider the case when $\alpha = 1$, here we have $\Phi(t) = e^{-\theta t}$, where $\theta = \tau^{-1}$. In this setting the hazard function is constant $h(t) = \theta$. The maximum likelihood estimate of θ is given by

$$\hat{\theta} = \frac{\sum_{i=1}^{m} v_i}{\sum_{i=1}^{m} x_i}, \tag{27}$$

which consists in the ratio between the sum of observable vaccination events and the total time at risk [22], i.e. the total time at risk of being vaccinated. It was estimated to be 17 vaccination events per 1000 person-days of exposure to vaccination, this means that on average it takes an individual 57 days from the start of the vaccination campaign to receive the vaccine.

Fig. 2 compares both the survival functions and cumulative hazard functions for the Kaplan-Meier estimates and the exponential model. We see that the exponential assumption fits the data poorly. These results show that there are two behaviours in the vaccination uptake, individuals that get the vaccine sooner, i.e. a greater vaccination (hazard) rate at the beginning, compared to the exponential model, or those who will get vaccinated much later, i.e. a decrease in hazard function as time goes on. This description does not suit the constant hazard function assumption as given by the exponential model. It instead suits a model in which at a given moment in time, for those not vaccinated yet, the time elapsed without vaccination influences their future vaccination outcome. We have previously described that the Mittag-Leffler distribution has such properties. Hence we will now consider the case where $0 < \alpha \leq 1$.

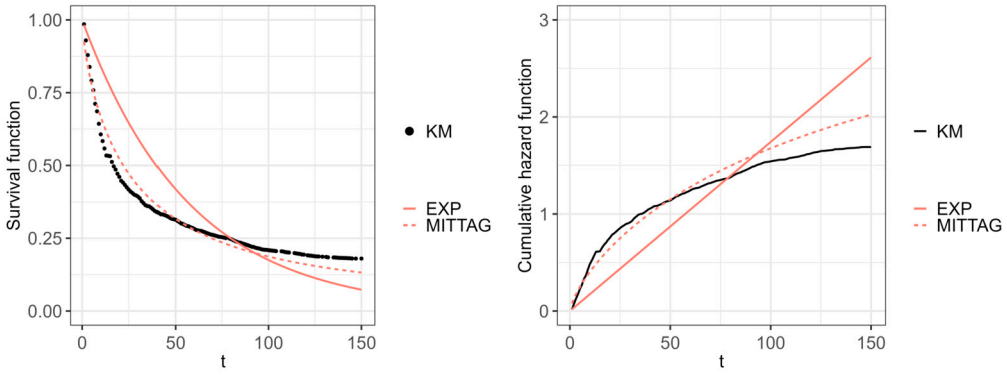

Fig. 3. Empirical, exponential and Mittag-Leffler survival functions for the times until vaccination (left). Empirical exponential and Mittag-Leffler cumulative hazard functions (right).

Table 1
Parameter estimates, 95% confidence interval for α, log-likelihood and AIC for the exponential ($\alpha = 1$) and Mittag-Leffler model (6). The confidence intervals were obtained via the profile likelihood function [26].

Model	α	α (95% CI)	θ	LogLikelihood	AIC
Exponential	1		0.017	-20700.16	41402.31
Mittag-Leffler (6)	0.7398	(0.7221,0.7574)	0.028	-19669.51	39343.02

There are no explicit formulas for the estimates of α and τ via the likelihood function (26) hence we use an optimisation approach by finding the minimum of the negative logarithm of (26)

$$LL(\alpha,\tau) = -\left(\sum_{i=1}^{m} v_i \log(\phi(x_i;\alpha,\tau)) + (1-v_i)\log(\Phi(x_i;\alpha,\tau))\right), \tag{28}$$

where $\Phi(t;\alpha,\tau) = E_{\alpha,1}(-(t/\tau)^\alpha)$ and $\phi(t;\alpha,\tau) = \frac{t^{\alpha-1}}{\tau^\alpha} E_{\alpha,\alpha}(-(t/\tau)^\alpha)$. Calculations of the Mittag-Leffler function were performed via the `MittagLeffleR` package [23]. Given that inference of α must be restricted to the interval $]0,1]$ and $\theta > 0$, we use the *L-BFGS-B* [24] method in the `optim` function. Where a lower and upper bound can be given for the accepted values for the parameters.

Fig. 3 displays the fitted Mittag-Leffler survival function, as given by formula (6), and cumulative hazard function compared to the results from empirical survival function and exponential fit. We observe that the Mittag-Leffler diplays a better agreement with the data when compared to the exponential distribution. This is corroborated by the AIC [25] found for both models. See Table 1. The Mittag-Leffler model displays a lower AIC, meaning that it is better suited to model these data when compared to the exponential model. There is a lower loss of information by selecting the Mittag-Leffler model. Furthermore we find a fractional order of $\alpha = 0.7398$, with 95% confidence interval (0.7221,0.7574), and a time scale parameter of $1/\tau = 0.028$. The confidence interval is narrow and does not contain 1 indicating that the history of an individual, as related to their vaccination status, will influence its future vaccination outcome, i.e. the longer an individual remains unvaccinated the more likely it is to continue to be unvaccinated. In this sense, the Mittag-Leffler model captures the swift initial vaccination uptake followed by an ever slower decaying vaccination rate. The fractional order α quantifies the degree of this memory effect, when compared to no memory ($\alpha = 1$), where a lower α suggests a stronger effect, i.e. faster vaccination uptake in the beginning and slower vaccination rates as time goes on, leaving more individuals unvaccinated as time goes on. In this sense, α measures the degree of hesitancy in the population towards getting vaccinated as time goes on.

4.1. Numerical method for the SIR model

We define $X_1(n) = S_{\Delta t}(n\Delta t)$ and $X_2(n) = I_{\Delta t}(n\Delta t)$, where $S_{\Delta t}(n\Delta t)$ and $I_{\Delta t}(n\Delta t)$ are the discrete approximations to $S(t)$ and $I(t)$ on the partition $n\Delta t$ with $n = 1, ..., N$ and step-size $\Delta t > 0$. The flux matrix Q we want to find is of the form

$$Q = \begin{bmatrix} 0 & Q_{1,2} & Q_{1,3} \\ 0 & 0 & Q_{2,3} \\ Q_{3,1} & Q_{3,2} & 0 \end{bmatrix} \tag{29}$$

Note that in system of equations (15) to (17) there is no flux from X_2 to X_1, and trivially no flux from a compartment to itself. Since $R(t) = 1 - S(t) - I(t)$ we group up all outfluxes and influxes associated with the R compartment along with those originating outside the system. These make up the third row and column of Q. The survival function associated with the Markovian flow from X_1 to X_2 is given by

$$\Theta_{1,2}(n,m) = \exp\left(-\int_{m\Delta t}^{n\Delta t} \beta I(s)\, ds \right) \tag{30}$$

This function depends on the integral of $I(t)$ over $[m\Delta t, n\Delta t]$, which is an integral over a variable of system of equations (15) to (17), and therefore unknown. However, $I(t)$ can be approximated by $X_2(n)$, where $n\Delta t = t$. We will address this issue at a later point.

The survival function associated with the Markovian outflow going outside the system coming from X_1 is given by

$$\Theta_{1,3}(n,m) = \exp\left(-\int_{m\Delta t}^{n\Delta t} \mu\, ds \right) = e^{-\mu\Delta t(m-n)}. \tag{31}$$

The non-Markovian survival function associated with the outflow from X_1 to compartment R is given by

$$\Phi_{1,3}(n) = E_{\alpha,1}\left(-\left(\frac{n\Delta t}{\tau} \right)^{\alpha} \right). \tag{32}$$

Finally, the survival function associated with the flow going outside the system and also to compartment R coming from X_2 is given by

$$\Theta_{2,3}(n,m) = \exp\left(-\int_{m\Delta t}^{n\Delta t} \mu + \gamma\, ds \right) = e^{-(\mu+\gamma)\Delta t(m-n)}. \tag{33}$$

The flows $Q_{3,1}$ and $Q_{3,2}$ can also be immediately computed

$$Q_{3,1}(n) = \int_{(n-1)\Delta t}^{n\Delta t} \mu\, ds + \delta_{0,n} S_0 = \mu\Delta t + \delta_{0,n} S_0, \tag{34}$$

which corresponds to the flow into X_1 coming from outside the system, where the first term of the right side corresponds to the number of births in a time interval of amplitude Δt and the second term is related to the initial injection of individuals, where $\delta_{0,n}$ denotes the Kronecker delta function and S_0 is the initial proportion of susceptible individuals. The influx in X_2 from outside the system is simply given by

$$Q_{3,2}(n) = \delta_{0,n} I_0, \tag{35}$$

where I_0 denotes the initial proportion of infected. Using all these ingredients we can compute $Q_{1,2}$, $Q_{1,3}$ and $Q_{2,3}$ using equation (13). We then have

$$Q_{1,2}(n) = \sum_{k=0}^{n-1} \big(\Theta_{1,2}(n-1,k)\Theta_{1,3}(n-1,k)\Phi_{1,3}(n-1-k)\big)(1-\Theta_{1,2}(n,n-1))Q_{3,1}(k), \tag{36}$$

$$\begin{aligned} Q_{1,3}(n) = &\sum_{k=0}^{n-1} \big(\Theta_{1,2}(n-1,k)\Theta_{1,3}(n-1,k)\Phi_{1,3}(n-1-k)\big)(1-\Theta_{1,2}(n,n-1))\Theta_{1,2}(n,n-1)Q_{3,1}(k) \\ &+ \sum_{k=0}^{n-1} \Theta_{1,2}(n,k)\Theta_{1,3}(n,k)(\Phi_{1,3}(n-1-k) - \Phi(n-k))Q_{3,1}(k) \end{aligned} \tag{37}$$

and

$$Q_{2,3}(n) = \sum_{k=0}^{n-1} \Theta_{2,3}(n-1,k)(1-\theta_{2,3}(n,n-1))(Q_{1,2}(k) + Q_{3,2}(k)). \tag{38}$$

Equations (36) and (37) depend on $\Theta_{1,2}$ which itself depends on the integral of system variable $I(t)$ over $[m\Delta, n\Delta t]$. Moreover, equation (38) depends on $Q_{1,2}$. Hence it is not possible to compute any of the non-trivial fluxes. To address this issue we approximate $\Theta_{1,2}$ as follows

$$\Theta_{1,2}(n,m) = \exp\left(-\int_{m\Delta t}^{n\Delta t} \beta I(s)\, ds \right) \tag{39}$$

$$\approx \exp\left(-\beta\Big(\frac{\Delta t}{2} X_2(m\Delta t) + \sum_{j=m+1}^{n-1} \Delta t X_2(j\Delta t) + \frac{\Delta t}{2} X_2(n\Delta t) \Big) \right), \tag{40}$$

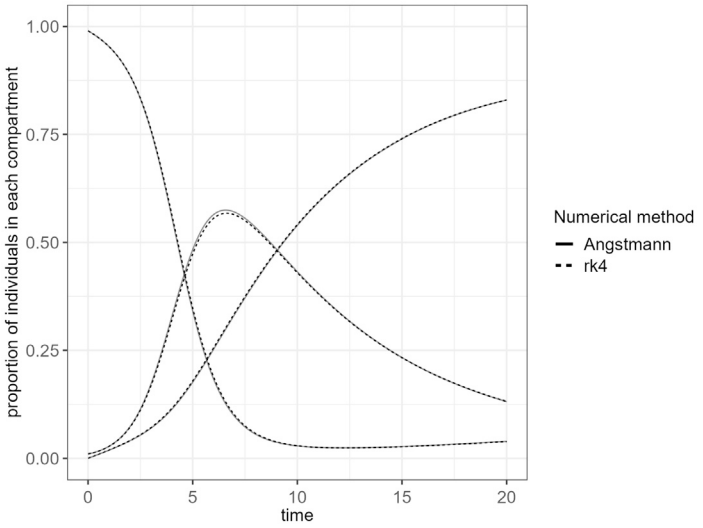

Fig. 4. Numerical simulations of the SIR model with vaccination using two distinct numerical methods. We perform numerical simulations using the Angstmann *ad hoc* method as described previously in this section and the Runge-Kutta fourth order method. We considered a time horizon of 20 days ($\Delta t = 0.1$, $n = 1, ..., 200$) with $\alpha = 1$, and $1/\tau = 0.017$, $\mu = 0.01$, $\beta = 1.2$, $\gamma = 1/7$, with initial conditions $S_0 = 0.99$ and $I_0 = 0.01$.

which corresponds to a trapezoidal approximation of the integral. $Q_{1,2}$ (n) depends on $\Theta_{1,2}(n)$, hence the last term in the summation in (40) will be unknown. To address this problem we can use a root finding algorithm at each step n in order to obtain $X_2(n)$. Using (12) we have

$$X_2(n-1) + Q_{1,2}(n; X_2(n)) + Q_{3,2}(n; X_2(n)) - Q_{2,3}(n; X_2(n)) - X_2(n) = 0, \tag{41}$$

where $X_2(0) = I_0$. We can find $X_2(n)$ at each iteration by finding the root of equation (41). To this end we use the `uniroot` [27] function to search for $X_2(n) \in [0, 1]$, $n = 1, ..., N$. In the same iteration, we can then directly calculate X_1 using (12)

$$X_1(n) = X_1(n-1) + Q_{3,1}(n) - Q_{1,2}(n) - Q_{1,3}(n), \tag{42}$$

where $X_1(0) = S_0$.

4.2. Numerical results

In this section, we present numerical simulations for the SIR model with vaccination using the method described in the previous section. We begin by comparing the *ad hoc* numerical method presented with a numerical method with high convergence order, in the case where $\alpha = 1$. In this way we can evaluate the results obtained using the *ad hoc* numerical method.

Fig. 4 compares the results obtained for the case when $\alpha = 1$ using two distinct numerical approaches. The approximations with solid lines employ the Angstmann method, as described previously in section 4.1. The solutions with dashed lines use a fourth-order Runge-Kutta numerical method [28]. There is agreement between both methods. The Runge-Kutta numerical method was implemented using the general solver `ode` from the `deSolve` package [29] in the `R` language and environment for statistical computing and graphics.

Next we want to study the stability of the equilibrium points found in section 3.1. Figs. 5a and 5b display simulations for the SIR model starting from the *disease free equilibrium* of susceptibles and $I_0 = 0.01$, while assuming $\mathcal{R} > 1$ and $\mathcal{R} < 1$, respectively. It suggests that when $\mathcal{R} > 1$ (in this particular case $\mathcal{R} = 2.5$), the system moves away from the *disease free equilibrium* and tends to an endemic equilibrium as $t \to \infty$, mimicking the behaviour found in the classical model. Moreover it appears to converge to the equilibrium points found in equation (18) for the susceptible proportion and equation (22) for the infected proportion, as indicated by the horizontal solid lines. When $\mathcal{R} < 1$ ($\mathcal{R} = 0.56$), we observe that the system converges to the *disease free equilibrium* as $t \to \infty$.

In the next simulations, our goal is to mimic an outbreak with characteristics similar to COVID-19 in a susceptible population while also incorporating vaccination. We consider an average infectious period of 7 days [30] ($\gamma = 1/7$) and natural mortality/birth rate $\mu = 0.01$. We use the values from Portugal, estimated in Section 4 to inform the vaccination process, with $1/\tau = 0.028$ and $\alpha = 0.7398$. We choose β such that the reproduction number is approximately 2.5 [31], resulting in $\beta = 1.2$. The system starts with $S_0 = 0.99$ and $I_0 = 0.01$. We use a step size of $\Delta t = 0.1$ and have $N = 200$ time steps, with a partition $n\Delta t$, $n = 1, ..., 250$ covering 25 days. A further Mittag-Leffler simulation is included with parameters $\alpha = 0.5$ with $1/\tau = 0.028$. Fig. 6 presents a side-by-side comparison of the simulations considered, along with the exponential case where $\alpha = 1$ and $\theta = 1/\tau = 0.017$ as obtained in Section 4.

During the early epidemic phase we observe a sharper decline in susceptibles, coinciding with a greater increase in recovered in both Mittag-Leffler simulations. With sharper changes in the simulation where $\alpha = 0.5$. Moreover, both Mittag-Leffler simulations display a lower peak of infections when compared to the exponential model. These results stem from the faster vaccination rate at the

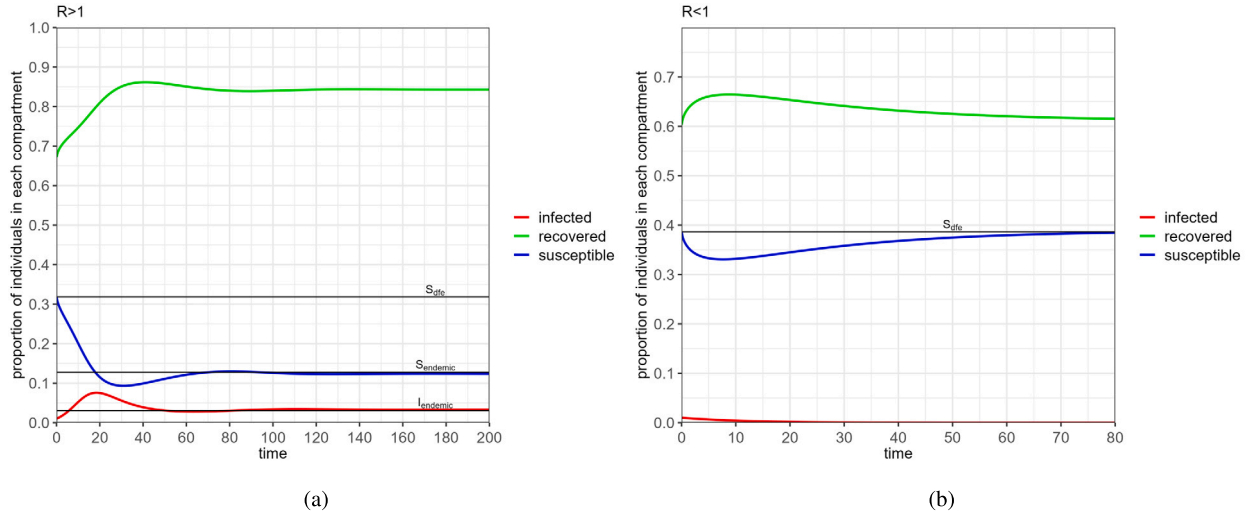

Fig. 5. (5a) Numerical simulation of the SIR model for a time horizon of 200 days ($\Delta t = 0.5$, n = 1,..., 400), considering $\beta = 1.2$, $\gamma = 1/7$ $\alpha = 0.7398$, $1/\tau = 0.028$ and $\mu = 0.01$, with $\mathcal{R} > 1$. Solid horizontal lines represent the *disease free equilibrium* and *endemic equilibrium* for the number of susceptible and infected individuals as given by equations (18) and (22). (5b). Numerical simulation of the SIR model for a time horizon of 80 days ($\Delta t = 0.2$, n = 1,..., 400), considering $\beta = 0.25$, $\gamma = 1/7$ $\alpha = 0.7398$, $1/\tau = 0.014$ and $\mu = 0.03$, with $\mathcal{R} < 1$. The solid horizontal line represents the *disease free equilibrium* of susceptible individuals. In both simulations we assumed $S_0 = S_{dfe}$ and $I_0 = 0.01$.

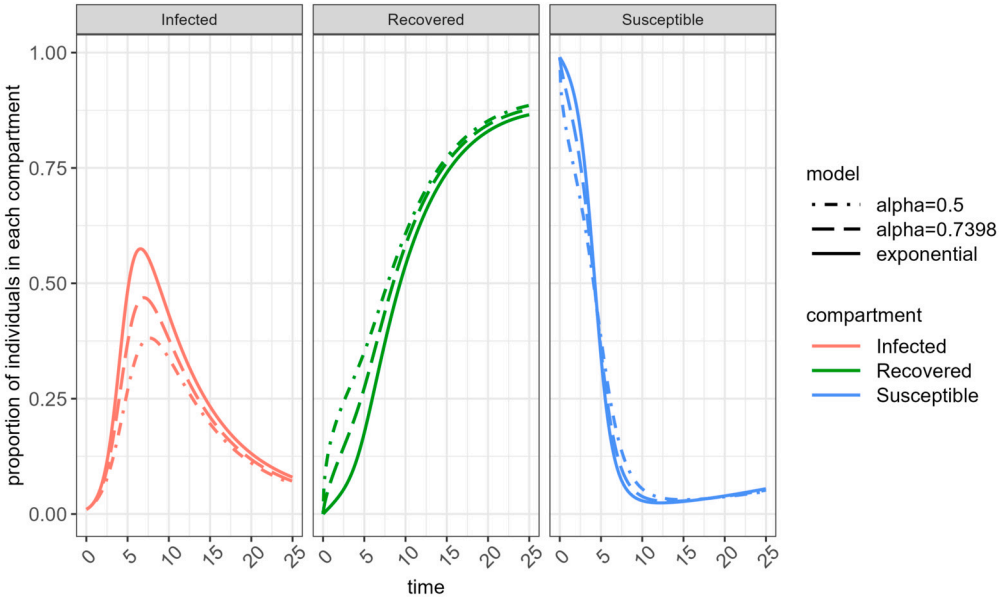

Fig. 6. Numerical simulations of the fractional order SIR model with vaccination. The number of susceptible, infected, and recovered individuals for each time step in the first 25 days is reported. A comparison is made between simulations with the exponential assumption ($\alpha = 1$ and $\theta = 0.017$) and Mittag-Leffler assumption ($\alpha = 0.7398$ with $1/\tau = 0.028$). These values are the maximum likelihood estimates obtained in Section 4. A further Mittag-Leffler simulation is included with parameters $\alpha = 0.5$ with $1/\tau = 0.028$.

start in the Mittag-Leffler model, i.e. a lower fractional order results in faster vaccination rates at the start as seen in the cumulative hazard rate displayed in Fig. 3. However, we also observe that as time progresses, the Mittag-Leffler simulations seem to get closer to the exponential simulation. This result can be in part due to the slowdown in vaccination uptake expected in the Mittag-Leffler model (see Fig. 3 right), leaving more individuals and unvaccinated as time goes on. Note that in the exponential model, vaccination uptake rate is constant and independent of the history of the individual.

5. Conclusion

With this work, we have shown the applicability and interpretability of fractional-order compartmental models for representing the vaccination roll-out, exemplified here by a non-Markovian removal process. This choice is motivated by the well-described waiting

times associated with this process, which follow the Mittag-Leffler distribution. The longer a particle is inside the compartment the more likely it is to not be removed, i.e., the longer an individual stays unvaccinated, the more likely it is to remain unvaccinated. This interpretation should excuse the use of these procedures to model non heavy-tail removal processes such as natural mortality. Thus, fractional order models should be used in a specific epidemiological context where some of the associated removal processes can be properly modelled by a Mittag-Leffler distribution, which should be supported by empirical data. For COVID-19 vaccination process, α was estimated to be equal to 0.7398 with 95% confidence interval (0.7221,0.7574) in Portugal during 2021. This indicates that vaccine uptake occurred more rapidly at the start and slower as time goes on. Through numerical simulations, we showed that these results greatly impact the dynamics of disease spread of COVID-19.

As future work, we intend to explore alternative, more robust numerical techniques beyond the one presented here, aiming to provide improved approximations for these problems while analysing their stability and convergence.

CRediT authorship contribution statement

Constantino Caetano: Conceptualization, Data curation, Formal analysis, Methodology, Software, Visualization, Writing – original draft, Writing – review & editing. **Luísa Morgado:** Conceptualization, Methodology, Supervision, Writing – review & editing. **Pedro Lima:** Conceptualization, Methodology, Supervision, Writing – review & editing. **Niel Hens:** Supervision, Writing – review & editing, Methodology. **Baltazar Nunes:** Supervision, Writing – review & editing.

Declaration of competing interest

We, the authors of the paper titled A fractional order SIR model describing hesitancy to the COVID-19 vaccination, declare that we have no financial or non-financial conflicts of interest that could influence the work presented in this paper.

Acknowledgements

The first author acknowledges FCT within the PhD grants “DOCTORATES 4 COVID”, grant number 2020.10172.BD. The second and third authors also acknowledge FCT within project UIDB/04621/2020 (Center for Computational and Stochastic Mathematics https://doi.org/10.54499/UIDB/04621/2020).

References

[1] C.N. Angstmann, B.I. Henry, A.V. McGann, A fractional-order infectivity and recovery sir model, Fractal Fract. 1 (1) (2017) 11, https://doi.org/10.3390/fractalfract1010011.
[2] A. Dokoumetzidis, P. Macheras, Fractional kinetics in drug absorption and disposition processes, J. Pharmacokinet. Pharmacodyn. 36 (2) (2009) 165–178, https://doi.org/10.1007/s10928-009-9116-x.
[3] A. Dokoumetzidis, R. Magin, P. Macheras, A commentary on fractionalization of multi-compartmental models, J. Pharmacokinet. Pharmacodyn. 37 (2) (2010) 203–207, https://doi.org/10.1007/s10928-010-9153-5.
[4] A. Dokoumetzidis, R. Magin, P. Macheras, Fractional kinetics in multi-compartmental systems, J. Pharmacokinet. Pharmacodyn. 37 (5) (2010) 507–524, https://doi.org/10.1007/s10928-010-9170-4.
[5] K. Diethelm, The Analysis of Fractional Differential Equations an Application-Oriented Exposition Using Differential Operators of Caputo Type, Springer, 2010.
[6] T. Sardar, S. Rana, J. Chattopadhyay, A mathematical model of Dengue transmission with memory, Commun. Nonlinear Sci. Numer. Simul. 22 (1–3) (2015) 511–525, https://doi.org/10.1016/j.cnsns.2014.08.009.
[7] K. Diethelm, A fractional calculus based model for the simulation of an outbreak of Dengue fever, Nonlinear Dyn. 71 (4) (2012) 613–619, https://doi.org/10.1007/s11071-012-0475-2.
[8] I.M. Batiha, A. Obeidat, S. Alshorm, A. Alotaibi, H. Alsubaie, S. Momani, M. Albdareen, F. Zouidi, S.M. Eldin, H. Jahanshahi, A numerical confirmation of a fractional-order covid-19 model’s efficiency, Symmetry 14 (12) (2022) 2583, https://doi.org/10.3390/sym14122583.
[9] K. Kozioł, R. Stanisławski, G. Bialic, Fractional-order sir epidemic model for transmission prediction of covid-19 disease, Appl. Sci. 10 (23) (2020) 8316, https://doi.org/10.3390/app10238316.
[10] S. Bushnaq, T. Saeed, D.F. Torres, A. Zeb, Control of covid-19 dynamics through a fractional-order model, Alex. Eng. J. 60 (4) (2021) 3587–3592, https://doi.org/10.1016/j.aej.2021.02.022.
[11] F. Ndaïrou, D.F. Torres, Mathematical analysis of a fractional covid-19 model applied to Wuhan, Spain and Portugal, Axioms 10 (3) (2021) 135, https://doi.org/10.3390/axioms10030135.
[12] C. Angstmann, A. Erickson, B. Henry, A. McGann, J. Murray, J. Nichols, A general framework for fractional order compartment models, SIAM Rev. 63 (2) (2021) 375–392, https://doi.org/10.1137/21m1398549.
[13] R.N. Pillai, On Mittag-Leffler functions and related distributions, Ann. Inst. Stat. Math. 42 (1) (1990) 157–161, https://doi.org/10.1007/bf00050786.
[14] C.N. Angstmann, B.I. Henry, A.V. McGann, A fractional order recovery sir model from a stochastic process, Bull. Math. Biol. 78 (3) (2016) 468–499, https://doi.org/10.1007/s11538-016-0151-7.
[15] T. Sardar, B. Saha, Mathematical analysis of a power-law form time dependent vector-borne disease transmission model, Math. Biosci. 288 (2017) 109–123, https://doi.org/10.1016/j.mbs.2017.03.004.
[16] H.W. Hethcote, D.W. Tudor, Integral equation models for endemic infectious diseases, J. Math. Biol. 9 (1) (1980) 37–47, https://doi.org/10.1007/bf00276034.
[17] H.W. Hethcote, H.W. Stech, P. van den Driessche, Stability analysis for models of diseases without immunity, J. Math. Biol. 13 (2) (1981) 185–198, https://doi.org/10.1007/bf00275213.
[18] R. Miller, On the linearization of Volterra integral equations, J. Math. Anal. Appl. 23 (1) (1968) 198–208, https://doi.org/10.1016/0022-247x(68)90127-3.
[19] C.N. Angstmann, B.I. Henry, B.A. Jacobs, A.V. McGann, An explicit numerical scheme for solving fractional order compartment models from the master equations of a stochastic process, Commun. Nonlinear Sci. Numer. Simul. 68 (2019) 188–202, https://doi.org/10.1016/j.cnsns.2018.07.009.
[20] R Core Team R, A Language and Environment for Statistical Computing, R Foundation for Statistical Computing, Vienna, Austria, 2022, https://www.R-project.org/.

[21] E.L. Kaplan, P. Meier, Nonparametric estimation from incomplete observations, J. Am. Stat. Assoc. 53 (282) (1958) 457–481, https://doi.org/10.1080/01621459.1958.10501452.
[22] D.R. Cox, D. Oakes, Analysis of Survival Data, Chapman and Hall, 1994.
[23] G. Gill, P. Straka, MittagLeffleR: using the Mittag-Leffler distributions in R, https://doi.org/10.6084/m9.figshare.6235898.v1, https://strakaps.github.io/MittagLeffleR/, May 2018.
[24] R.H. Byrd, P. Lu, J. Nocedal, C. Zhu, A limited memory algorithm for bound constrained optimization, SIAM J. Sci. Comput. 16 (5) (1995) 1190–1208, https://doi.org/10.1137/0916069, arXiv:https://doi.org/10.1137/0916069.
[25] H. Akaike, A new look at the statistical model identification, IEEE Trans. Autom. Control 19 (6) (1974) 716–723, https://doi.org/10.1109/tac.1974.1100705.
[26] N. Hens, Modeling Infectious Disease Parameters Based on Serological and Social Contact Data a Modern Statistical Perspective, Springer, 2012.
[27] R.P. Brent, Algorithms for minimization without derivatives, Dover, 2013.
[28] J.C. Butcher, On Runge-Kutta processes of high order, J. Aust. Math. Soc. 4 (2) (1964) 179–194, https://doi.org/10.1017/s1446788700023387.
[29] K. Soetaert, T. Petzoldt, R.W. Setzer, Solving differential equations in R: package deSolve, J. Stat. Softw. 33 (9) (2010) 1–25, https://doi.org/10.18637/jss.v033.i09.
[30] European Centre for Disease Prevention and Control, Transmission of covid-19, https://www.ecdc.europa.eu/en/infectious-disease-topics/z-disease-list/covid-19, 2022. (Accessed 26 January 2024).
[31] Y. Liu, J. Rocklöv, The reproductive number of the delta variant of sars-cov-2 is far higher compared to the ancestral sars-cov-2 virus, J. Travel Med. 28 (7) (Aug 2021), https://doi.org/10.1093/jtm/taab124.